Research Article | Vol. 11, No. 11 / 1 November 2020 / Biomedical Optics Express 6528
Biomedical Optics EXPRESS

Differentiation of burn wounds in an *in vivo* porcine model using terahertz spectroscopy

Omar B. Osman,[1] Timothy Jack Tan,[1] Sam Henry,[2] Adelaide Warsen,[3] Navid Farr,[4] Abbi M. McClintic,[4] Yak-Nam Wang,[4] Saman Arbabi,[3] and M. Hassan Arbab[1,4,*]

[1]*Department of Biomedical Engineering, Stony Brook University, Stony Brook, NY 11794, USA*
[2]*Computer Engineering and Systems Department, University of Washington, Tacoma, WA 98402, USA*
[3]*Burn Center and Division of Plastic Surgery, Department of Surgery, University of Washington, Seattle, WA 98104, USA*
[4]*Applied Physics Laboratory, University of Washington, Seattle, WA 98105, USA*
[*]*hassan.arbab@stonybrook.edu*

Abstract: The accuracy of current burn triage techniques has remained between 50-70%. Accordingly, there is a significant clinical need for the quantitative and accurate assessment of partial-thickness burn injuries. Porcine skin represents the closest animal model to human skin, and is often used in surgical skin grafting procedures. In this study, we used a standardized *in vivo* porcine burn model to obtain terahertz (THz) point-spectroscopy measurements from burns with various severities. We then extracted two reflection hyperspectral parameters, namely spectral area under the curve between approximately 0.1 and 0.9 THz (−10 dB bandwidth in each spectrum), and spectral slope, to characterize each burn. Using a linear combination of these two parameters, we accurately classified deep partial- and superficial partial-thickness burns (p = 0.0159), compared to vimentin immunohistochemistry as the gold standard for burn depth determination.

1. Introduction

Burn injuries result in over 450,000 emergency room visits per year [1]. Traditionally, thermal injuries are categorized from first-degree to third-degree burns. First-degree, or superficial burns, only affect the epidermis and will typically heal with minimal intervention. Third-degree burns, or full-thickness burns, damage the entirety of the dermis and require surgical excision and grafting. Second-degree burns, where the damage is contained within the dermis, can be further classified into two groups: superficial partial-thickness and deep partial-thickness burns. Similar to first-degree burns, superficial partial-thickness burns also will heal spontaneously, whereas deep partial-thickness burns eventually will progress into full-thickness burns and require surgical intervention. Accurate assessment of burn injuries is therefore critical, in cases requiring surgical intervention, as early excision results in better overall healing outcomes [2]. Although determination of burn severity often is performed by experienced burn care physicians, the accuracy rate of burn triage, based on the depth of dermal damage, can be as low as 50-70% in second-degree burns [3].

Many techniques, such as laser Doppler imaging (LDI) [4], polarization-sensitive optical coherence tomography (PS-OCT) [5], photoacoustic imaging [6], and multispectral imaging [7], have been proposed to provide quantitative methods for objective assessment of burn depth. Laser doppler is a non-contact method that measures perfusion in the burn area, but has not achieved clinical adoption because LDI instruments are not user-friendly and can be subject to inconsistencies and variability when imaging uneven surfaces or in patients with comorbidities [8]. PS-OCT provides cross-sectional imaging from backscattered illumination with additional contrast from damaged collagen fibers that have lost their structural arrangement due to thermal

#397792 https://doi.org/10.1364/BOE.397792
Journal © 2020 Received 18 May 2020; revised 26 Jul 2020; accepted 24 Aug 2020; published 19 Oct 2020

Biomedical Optics EXPRESS

insult. However, the field of view of OCT imaging is usually much smaller than clinically practical for burn management. Multi-spectral imaging has also shown some promise in determining burn depths by measuring the reflectance at a specific wavelength using optical filters [7].

Terahertz time-domain spectroscopy (THz-TDS) is emerging as an effective tool in burn assessment because of the unique properties of skin and other biological tissue in the terahertz (THz) regime [9]. THz waves (wavelength between 3 mm and 10 μm) are nonionizing and highly absorptive in polar liquids (i.e. water) [10], thus THz-TDS is sensitive to small changes in water content. Additionally, the sizes of adnexal skin structures (such as glands and follicles) are on the same scale as THz wavelengths. As a result, electromagnetic scattering from skin structures can be an additional source of contrast [11] as granular, volume and rough-surface scattering are wavelength dependent [12–14]. Previous THz studies have used narrow band detection schemes (500 GHz ± 125GHz) for THz imaging of *ex vivo* porcine burns [15]. However, due to the limited bandwidth, the effect of scattering from skin structures could not be detected. Also, because the study was performed *ex vivo*, the physiological and anti-inflammatory response to a burn injury could not be observed. Further *in vivo* studies in rat models used narrow band THz imaging to show the formation and dissipation of edema in response to a thermal injury [16]. Dual-modality studies with co-registered magnetic resonance imaging also confirmed that hydration plays a major role in the signal contrast of THz burn imaging [17,18]. Broadband THz *in vivo* studies in rats have shown the sensitivity of time-domain spectroscopy modality to different grades of burn injury, not only based on the higher THz reflectivity of partial-thickness burns, but also due to the change in density of skin structures post burn [11,19,20]. However, the major limitation of the rat studies for assessment of burn depth is that the anatomy and physiology of rat skin is significantly different from human skin.

The pathophysiology of wound healing in burn injuries is a complex process. Porcine skin is an ideal animal model for burn studies because of its physiological and anatomical resemblance to human skin. Humans and swine have firmly attached skin architecture, thick dermis and epidermis, and sparsely distributed hair, whereas rodents have loosely attached skin, thin dermal and epidermal layers, and dense hair [21]. Moreover, the mechanism for wound healing in humans and swine is reepithelialization, whereas wound healing in rodents is through a contraction mechanism. Additionally, the genomic and proteomic responses of inflammatory diseases, such as burn and sepsis, are much closer between swine and humans, and distinctly different in rodents [22]. Therefore, porcine models are accepted as the appropriate animal model to capture the wound healing and dynamic response of skin burns for future clinical translation.

In this paper, we show that the THz spectral parameters, which we have shown to be accurate in characterizing rat burns [11], are also able to differentiate burn severities in porcine burns. We used a standardized protocol to induce burns with multiple severities, and a commercial THz system to obtain point spectroscopy measurements of each burn. We used vimentin immunohistochemistry (IHC) as the gold standard to determine the burn depth. We show that a linear combination of two THz spectral parameters, namely spectral area to represent reflectivity and spectral slope to represent scattering, can classify deep partial- and superficial partial-thickness burns accurately (p = 0.0159). The new spectroscopic method for the classification of porcine burns with THz-TDS is an important preliminary step towards clinical translation of THz spectral imaging for burn wound assessment.

2. Materials and methods

2.1. Animal model

The experimental protocol used in this study was reviewed and approved by the Institutional Animal Care and Use Committee at the University of Washington. After induction of anesthesia, burns were created on Landrace Yorkshire cross pigs (N = 3, 12 weeks age, male, 40 kg). Burn injuries were created using a standardized induction protocol described by Cuttle et al. [23].

Biomedical Optics EXPRESS

Shown in Fig. 1(a), a "hot water bottle" (500 ml Pyrex laboratory Schott Duran bottle) with the glass bottom removed and replaced with plastic wrap fastened with heat resistant tape was filled with 300 ml of deionized water heated to 92°C. The plastic wrap conforms to the anatomical contours of the body, resulting in even surface contact. Three dorsal locations were chosen along the midline for burn induction with three contralateral sites for healthy skin (control). Each burn site received 10, 15, or 20 seconds exposure to 92°C, respectively creating superficial partial-thickness, deep partial-thickness, and full-thickness burns, for a total of 3 burns per experimental arm. After burn induction, the necrotic epidermis was debrided in accordance with clinical wound management per the protocol described in [23]. Each circular wound was 8 cm in diameter, and approximately 10 cm apart. Figure 1(b-d) shows a representative set of the histological sections for normal and burn tissues obtained by vimentin immunohistochemistry.

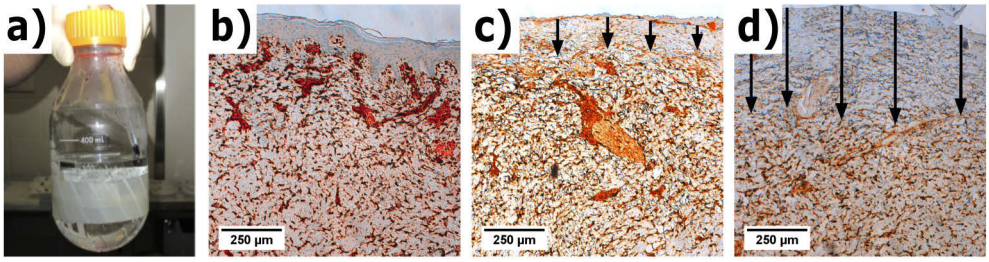

Fig. 1. (a) shows visual images of the "hot water bottle" device before use. Vimentin IHC section slides are shown from a representative (b) normal, (c) superficial partial-thickness, and (d) deep partial-thickness burn. The arrows indicate the depth of the burn injury.

2.2. Histopathology

Vimentin IHC is based on the labeling of an intermediate filament protein that is ubiquitous among mesenchymal, melanocytes and Langerhans' cells [24]. We used the well-established vimentin IHC assay because antisera testing can label the exact depth of thermal tissue damage in burns [24]. Arrows in Fig. 1(b-d) show the burn depth, according to the loss of vimentin-positive stained cells in the dermis. The depth of the burn was measured in sections labeled for vimentin using a stereological approach. Briefly, vertical uniform random sampling of each specimen was used to obtain unbiased, isotropic sections to make depth measurements [25]. Parallel lines with an interline distance of 1500 µm were randomly overlaid on rotated images of each slide. Orthogonal lines to the surface of the epidermis were drawn from these intersections to measure the depth [25]. From these measurements, the arithmetic and harmonic thickness were calculated to account for overestimation of thickness due to variation in sectioning angles.

2.3. THz measurements

Our measurements were completed using a commercial THz-TDS unit (K15, Menlo Systems Inc, Newton, New Jersey, USA) mounted on a flexible platform. The pulsed system uses a mode-locked <90 femtosecond (fs) fiber laser operating at 1560 nm. The optical pulse is split into a pump and probe beam. Each beam is focused onto a photoconductive antenna to emit and detect broadband THz radiation. The THz beam generated by the photoconductive antenna is diverging, so it was collimated and then focused with a 50 mm focusing lens. The spot size of the beam at the focal point was 1-2 mm. Illustrated in Fig. 2(a), the emitter and receiver were mounted at 37° relative to normal incidence. The emitting and detecting modules were placed inside a plastic enclosure and purged with nitrogen. Figure 2(b) shows the enclosure mounted on a cantilevered c-arm and anchored to the operating table with vertical motor control. THz measurements were obtained approximately 20-30 minutes after burn induction and each

Biomedical Optics EXPRESS

measurement took approximately 5 minutes to complete. At the time of measurement, the operating table was moved close to the porcine subject on an adjacent operating table, and the THz enclosure was lowered onto the selected spot. We first measured the THz reflection spectra at the center of each burn and subsequently measured the edge by laterally shifting the setup by approximately 4 cm. Reflectivity data were collected in the time domain, with a total scan range of 52 picoseconds (ps) and time resolution of 0.195 ps. All pulses were gated with a 178 ps Hamming window and Fourier transformed using a 512-point FFT. The maximum frequency that can be extracted is therefore 2.56 THz with the frequency resolution of 0.01 THz.

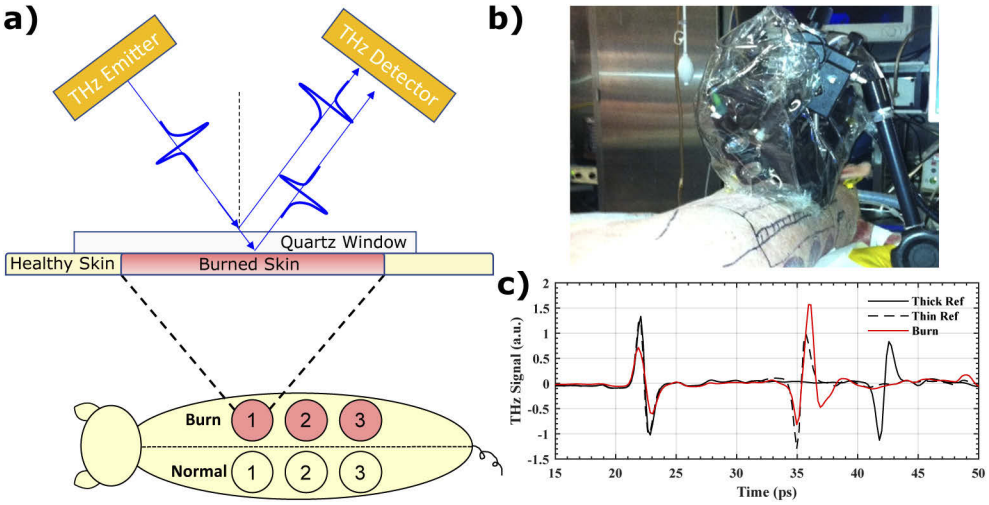

Fig. 2. (a) shows a schematic drawing of the burn sites and the contralateral healthy controls along with the typical wave incidence and propagation through the quartz window and the sample. (b) A picture of the THz-TDS system is shown mounted over an animal subject in the operating room. (c) THz-TDS signals of the thick window reference (black-solid), thin window reference (black-dashed) and a representative burn (red-solid).

A quartz measurement window was used as part of a self-calibration procedure [19,26] and to ensure smooth contact with the porcine skin sample. Illustrated in the schematic from Fig. 2(a) and the THz-TDS signals in Fig. 2(c), the raw THz waveform typically contains two pulses, one from the air-quartz interface, and another from the quartz-sample interface. The first pulse from the quartz window served as a phase and amplitude reference to which all subsequent THz pulses were normalized in amplitude and aligned in time prior to Fourier transform. A reference measurement was taken without a sample, representing the reflection from the quartz-air interface. We also obtained a separate reference measurement from a thick slab of quartz (approximately 1.566 mm) and subtracted it from the thin quartz reference (approximately 1.044 mm), to calculate a Differential Reference. This step removes the background ringing due to air-quartz reflection from the second reflection from the quart-air interface [19,26]. The same subtraction operation was performed on sample measurements to remove the background signal.

2.4. Signal processing

Figure 3(a) describes the signal processing steps in which the reference measurements were used to calculate the spectral parameters. A split cosine window was applied to the first and last 20 points of the time-domain signal of the differential reference and background removed-sample before fast Fourier transformation (FFT). Sample measurements that were taken from the same burn were averaged together in the frequency domain.

Biomedical Optics EXPRESS

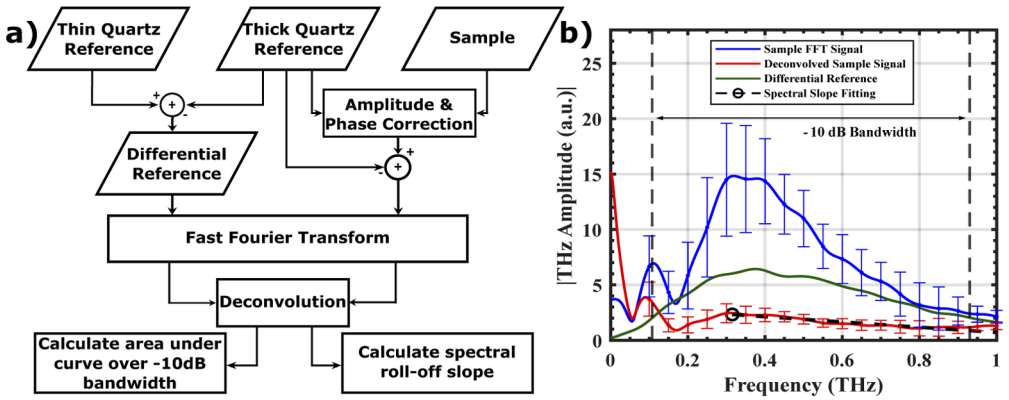

Fig. 3. (a) shows the signal processing flowchart and (b) shows a representative sample reflectivity after the FFT and deconvolution by Differential Reference. Vertical dashed lines show the −10 dB bandwidth used for the spectral area and slope calculations in the THz amplitude spectrum.

We calculated the spectral parameters by first determining the frequency bins of the −10 dB bandwidth in the THz amplitude spectrum of the differential reference, shown by the vertical black dotted lines in Fig. 3(b). This was done by selecting the upper and lower frequencies bins where the THz signal approached −10 dB with respect to the maximum THz amplitude. We then deconvolved the sample signal by the quartz reference. The area under the curve was determined within the −10 dB bandwidth and the roll-off spectral slope, shown by the black-dashed line in Fig. 3(b) was calculated by a least-squares linear fit between the maximum amplitude (black circle) to the upper −10 dB frequency bin. A unitless hyperspectral parameter, dubbed Z-metric, was calculated by

$$Z = a \cdot SA + b \cdot SS. \tag{1}$$

where a and b are coefficients between 0 and 1, SA is the spectral area, and SS is the spectral slope. The coefficients, a and b, were optimized for classification of burns greater than 350 µm. The search domain for the optimization of a and b was between 0 and 1, with increments in the fourth decimal position, until the maximal distance between the two classes was achieved. We selected 350 µm depth because it would ensure that the epithelium was damaged (deeper than superficial burns) but many of the adnexal structures in the dermis were still healthy. Adnexal structures, such as hair follicles, are sources of appendageal keratinocytes that will migrate and promote reepithelialization.

3. Results

3.1. Burn depth variability

Figure 4(a) shows the average burn depth for each induction protocol at the center and edge of the burns, determined by the vimentin IHC assay. With increasing exposure time from 10 to 15 and 20 seconds, the average burn depth increases at both the center and edge of each experimental arm. The error bars, representing the standard deviation of the mean, show large variability in burn depths across exposure times. This variability in burn depth from each condition is likely a result of the burn's anatomic location, as explained in Fig. 1(a). Figure 4(b) shows that burn depth increased in cranial sites as compared to middle and caudal positions. This is likely due to hard tissue, such as bone or cartilage, beneath the skin at those sites, which provide more gravitational support to the burn device and compression to the skin. This effect can result in more force and thus deeper burns [27]. Burn depth was also found to be deeper at the center of

Biomedical Optics EXPRESS

the burn than at the edge, which can be explained by dissipation of thermal energy toward the healthy skin. Although the standardized protocol for burn induction created a wide range of burn depth variation, in the following section we will show that the THz spectroscopic measurements were able to accurately characterize the burn depth.

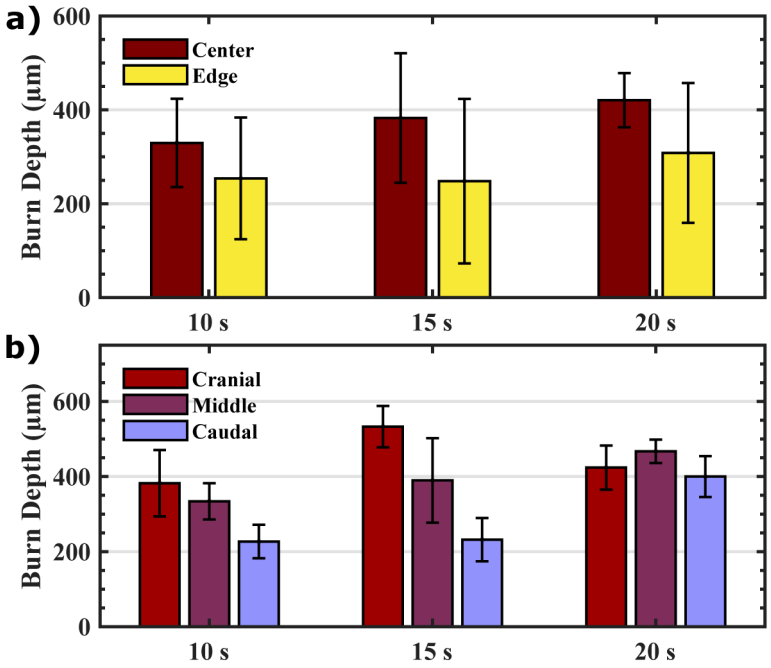

Fig. 4. (a) shows the average burn depth for various exposure times at the center and edge of the burn area, (b) compares the burn depth at the center of the burn from three anatomical locations (cranial, middle, and caudal) for each burn condition. Error bars represent standard deviation.

3.2. *Spectral parameters and classification*

Figure 5(a) shows the linear relationship between the calculated spectral parameters and burn depth from histology. By combining these two parameters into a Z-metric (Eq. 1, where $a = 0.7475$ and b = 0.0202), as it is shown in Fig. 5(b), we were able to see improved classification accuracy (Mann-Whitney U-Test, $p = 0.0159$) between deep partial- and superficial partial-thickness burns. We used the Mann-Whitney U-Test over the Student's t-test because there is no population data available for THz reflectivity in porcine burns to determine the distribution. Assuming that THz measurements from deep partial- and superficial partial-thickness burn injuries have similar population distributions, the Mann-Whitney U-test is appropriate to test the null hypothesis. Also, interestingly, as compared to our previous work in rat models [11, 28], the relatively smaller weight for spectral slopes represented by the *b* coefficient is in agreement with the smaller density of hair follicles and thus less scattering in porcine skin.

Biomedical Optics EXPRESS

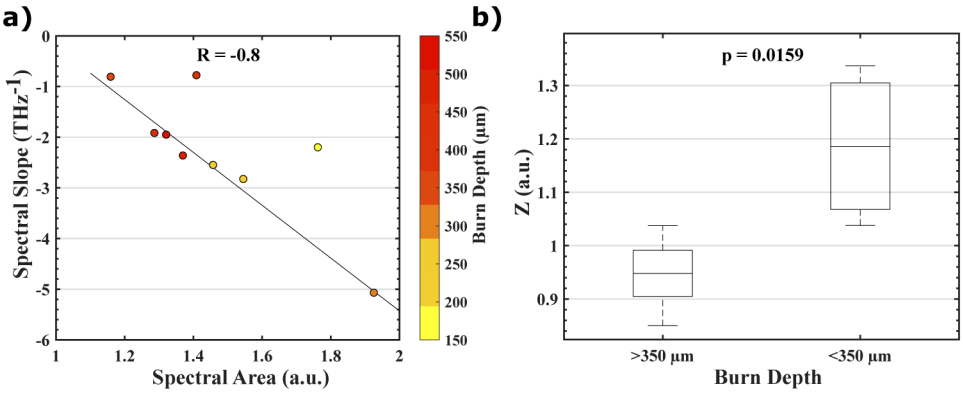

Fig. 5. (a) shows a linear relationship (illustrated by the black least squares line in the scatter plot) between spectral area and spectral slope with the burn depth represented by the colored markers and the color axis. (b) A linear combination of spectral area and spectral slope, defined by the Z value in Eq. (1), shows statistically significant classification of superficial partial- and deep partial-thickness burns (Mann-Whitney U-Test, p = 0.0159).

4. Conclusion

We presented an *in vivo* THz-TDS study for characterization of burn injuries in a porcine model. We used a standardized burn protocol that produces uniform burns by allowing a hot water bottle to conform to the contours of the animal's skin. After burn induction, we obtained point spectroscopy measurements with a commercial THz-TDS system modified to be mounted on a cantilevered c-arm for use inside an operating room. We showed that by using spectral parameters that represent reflectivity and electromagnetic scattering in the measured THz-TDS signal we can classify burn depth, as determined by the vimentin assay as the histopathological control. Future work includes assessment of burn injuries using *in vivo* THz spectral imaging and long-term survival studies, in which the final healing outcome of each partial-thickness burn can be determined. THz spectral imaging in porcine burn models will pave the way to creating a translational imaging modality that will help physicians rapidly and accurately treat burn victims.

Funding

National Institute of General Medical Sciences (R01GM112693).

Acknowledgements

The authors would like to thank the Department of Comparative Medicine at the University of Washington for all veterinary services and animal husbandry during these animal studies. Research reported in this publication was supported by the National Institute of General Medical Sciences of the National Institutes of Health under award number R01GM112693.

Disclosures

P: MHA discloses intellectual property owned by the University of Washington, US Patent No. US9295402B1.

References

1. American Burn Association, "Burn incidence fact sheet [online]," (2015).
2. Y. S. Ong, M. Samuel, and C. Song, "Meta-analysis of early excision of burns," Burns **32**(2), 145–150 (2006).
3. B. S. Atiyeh, S. W. Gunn, and S. N. Hayek, "State of the art in burn treatment," World J. Surg. **29**(2), 131–148 (2005).

Biomedical Optics EXPRESS

4. A. J. A. Holland, H. C. O. Martin, and D. T. Cass, "Laser Doppler imaging prediction of burn wound outcome in children," Burns **28**(1), 11–17 (2002).
5. B. H. Park, C. E. Saxer, S. M. Srinivas, J. S. Nelson, and J. F. de Boer, "In vivo burn depth determination by high-speed fiber-based polarization sensitive optical coherence tomography," J. Biomed. Opt. **6**(4), 474 (2001).
6. Z. Wu, F. Duan, J. Zhang, S. Li, H. Ma, and L. Nie, "In vivo dual-scale photoacoustic surveillance and assessment of burn healing," Biomed. Opt. Express **10**(7), 3425–3433 (2019).
7. J. E. Thatcher, W. Li, Y. Rodriguez-Vaqueiro, J. J. Squiers, W. Mo, Y. Lu, K. D. Plant, E. Sellke, D. R. King, W. Fan, J. A. Martinez-Lorenzo, and J. M. DiMaio, "Multispectral and photoplethysmography optical imaging techniques identify important tissue characteristics in an animal model of tangential burn excision," J Burn Care Res **37**(1), 38–52 (2016).
8. J. E. Thatcher, J. J. Squiers, S. C. Kanick, D. R. King, Y. Lu, Y. Wang, R. Mohan, E. W. Sellke, and J. M. DiMaio, "Imaging techniques for clinical burn assessment with a focus on multispectral imaging," Adv. wound care **5**(8), 360–378 (2016).
9. E. Pickwell and V. P. Wallace, "Biomedical applications of terahertz technology," J. Phys. D: Appl. Phys. **39**(17), R301–R310 (2006).
10. J. T. Kindt and C. A. Schmuttenmaer, "Far-infrared dielectric properties of polar liquids probed by femtosecond terahertz pulse spectroscopy," J. Phys. Chem. **100**(24), 10373–10379 (1996).
11. M. H. Arbab, D. P. Winebrenner, T. C. Dickey, A. Chen, M. B. Klein, and P. D. Mourad, "Terahertz spectroscopy for the assessment of burn injuries in vivo," J. Biomed. Opt. **18**(7), 077004 (2013).
12. O. B. Osman and M. H. Arbab, "Mitigating the effects of granular scattering using cepstrum analysis in terahertz time-domain spectral imaging," PLoS One **14**(5), e0216952 (2019).
13. Y. Shen, P. Taday, and M. Pepper, "Elimination of scattering effects in spectral measurement of granulated materials using terahertz pulsed spectroscopy," Appl. Phys. Lett. **92**(5), 051103 (2008).
14. S. Schecklman, L. M. Zurk, S. Henry, and G. P. Kniffin, "Terahertz material detection from diffuse surface scattering," J. Appl. Phys. **109**(9), 094902 (2011).
15. Z. D. Taylor, R. S. Singh, M. O. Culjat, J. Y. Suen, W. S. Grundfest, H. Lee, and E. R. Brown, "Reflective terahertz imaging of porcine skin burns," Opt. Lett. **33**(11), 1258–1260 (2008).
16. P. Tewari, C. P. Kealey, D. B. Bennett, N. Bajwa, K. S. Barnett, R. S. Singh, M. O. Culjat, A. Stojadinovic, W. S. Grundfest, and Z. D. Taylor, "In vivo terahertz imaging of rat skin burns," J. Biomed. Opt. **17**(4), 040503 (2012).
17. N. Bajwa, S. Sung, D. B. Ennis, M. C. Fishbein, B. N. Nowroozi, D. Ruan, A. Maccabi, J. Alger, M. A. S. John, and W. S. Grundfest, "Terahertz imaging of cutaneous edema: correlation with magnetic resonance imaging in burn wounds," IEEE Trans. Biomed. Eng. **64**(11), 2682–2694 (2017).
18. P. Tewari, J. Garritano, N. Bajwa, S. Sung, H. Huang, D. Wang, W. Grundfest, D. B. Ennis, D. Ruan, and E. Brown, "Methods for registering and calibrating in vivo terahertz images of cutaneous burn wounds," Biomed. Opt. Express **10**(1), 322–337 (2019).
19. M. H. Arbab, T. C. Dickey, D. P. Winebrenner, A. Chen, M. B. Klein, and P. D. Mourad, "Terahertz reflectometry of burn wounds in a rat model," Biomed. Opt. Express **2**(8), 2339–2347 (2011).
20. M. H. Arbab, T. C. Dickey, D. P. Winebrenner, A. Chen, and P. D. Mourad, "Characterization of burn injuries using terahertz time-domain spectroscopy," in *Advanced Biomedical and Clinical Diagnostic Systems IX*, vol. 7890 (International Society for Optics and Photonics, 2011), p. 78900Q.
21. A. Abdullahi, S. Amini-Nik, and M. Jeschke, "Animal models in burn research," Cell. Mol. Life Sci. **71**(17), 3241–3255 (2014).
22. J. Seok, H. S. Warren, A. G. Cuenca, M. N. Mindrinos, H. V. Baker, W. Xu, D. R. Richards, G. P. McDonald-Smith, H. Gao, and L. Hennessy, "Genomic responses in mouse models poorly mimic human inflammatory diseases," Proc. Natl. Acad. Sci. **110**(9), 3507–3512 (2013).
23. L. Cuttle, M. Kempf, G. E. Phillips, J. Mill, M. T. Hayes, J. F. Fraser, X.-Q. Wang, and R. M. Kimble, "A porcine deep dermal partial thickness burn model with hypertrophic scarring," Burns **32**(7), 806–820 (2006).
24. L. B. Nanney, B. A. Wenczak, and J. B. Lynch, "Progressive burn injury documented with vimentin immunostaining," J. Burn Care Rehabil. **17**(3), 191–198 (1996).
25. Y.-N. Wang, K. Lee, and W. R. Ledoux, "Histomorphological evaluation of diabetic and non-diabetic plantar soft tissue," Foot Ankle Int. **32**(8), 802–810 (2011).
26. R. M. Woodward, B. E. Cole, V. P. Wallace, R. J. Pye, D. D. Arnone, E. H. Linfield, and M. Pepper, "Terahertz pulse imaging in reflection geometry of human skin cancer and skin tissue," Phys. Med. Biol. **47**(21), 3853–3863 (2002).
27. A. J. Singer, B. R. Taira, R. Anderson, S. A. McClain, and L. Rosenberg, "Does pressure matter in creating burns in a porcine model?" J. Burn. Care & Res. **31**(4), 646–651 (2010).
28. M. H. Arbab, D. P. Winebrenner, T. Dickey, M. Klein, A. Chen, and P. Mourad, "A Noninvasive Terahertz Assessment of 2nd and 3rd Degree Burn Wounds," in *Conference on Lasers and Electro-Optics 2012*, OSA Technical Digest (online), https://10.1364/CLEO_SI.2012.CTu3B.3 (Optical Society of America, 2012).